APPLIED PHYSICS REVIEWS

$LiNbO_3$: A photovoltaic substrate for massive parallel manipulation and patterning of nano-objects

M. Carrascosa,[1] A. García-Cabañes,[1] M. Jubera,[1] J. B. Ramiro,[2] and F. Agulló-López[3]
[1]*Dept. Física de Materiales, Universidad Autónoma de Madrid, Madrid 28049, Spain*
[2]*Dept. Mecánica de Fluidos y Propulsión Aeroespacial, Universidad Politécnica de Madrid, Madrid 28040, Spain*
[3]*Centro de Microanálisis de Materiales (CMAM), Universidad Autónoma de Madrid, Madrid 28049, Spain*

(Received 17 April 2015; accepted 21 July 2015; published online 20 October 2015)

The application of evanescent photovoltaic (PV) fields, generated by visible illumination of Fe:$LiNbO_3$ substrates, for parallel massive trapping and manipulation of micro- and nano-objects is critically reviewed. The technique has been often referred to as photovoltaic or photorefractive tweezers. The main advantage of the new method is that the involved electrophoretic and/or dielectrophoretic forces do not require any electrodes and large scale manipulation of nano-objects can be easily achieved using the patterning capabilities of light. The paper describes the experimental techniques for particle trapping and the main reported experimental results obtained with a variety of micro- and nano-particles (dielectric and conductive) and different illumination configurations (single beam, holographic geometry, and spatial light modulator projection). The report also pays attention to the physical basis of the method, namely, the coupling of the evanescent photorefractive fields to the dielectric response of the nano-particles. The role of a number of physical parameters such as the contrast and spatial periodicities of the illumination pattern or the particle deposition method is discussed. Moreover, the main properties of the obtained particle patterns in relation to potential applications are summarized, and first demonstrations reviewed. Finally, the PV method is discussed in comparison to other patterning strategies, such as those based on the pyroelectric response and the electric fields associated to domain poling of ferroelectric materials.
 [http://dx.doi.org/10.1063/1.4929374]

TABLE OF CONTENTS

I. INTRODUCTION

The field of trapping and manipulation of micro- and nano-objects, including molecules, living cells, bacteria, and material crystallites or powders, is very active and offers interesting possibilities in a variety of applications ranging from nano-technology to photonics, biology, and biomedicine.[1–3] As an example, one may quote spatial localization and orientation of nano-objects, structural and biological modification of living organisms, and organization of large assemblies in accordance with imposed external patterns. The topic is also a fundamental issue in microfluidic technology.[4] Several strategies have been proposed and/or

developed for such purposes that rely on optical, electrical, electrokinetical, and pyroelectric methods. Well-known examples of such strategies are atomic force microscopy (AFM) and related microscopy methods,[5–7] and optical trapping by focused light beams[8,9] (optical tweezers). A main shortcoming of these techniques is that they cannot offer high resolution and high throughput at the same time, although new strategies such as holographic tweezers,[1,10] are able to overcome this problem. Another useful approach uses the electrophoretic or dielectrophoretic forces associated to the imposed electric field patterns intended to generate the final arrangement of the nano-objects.[11–14] This strategy can be easily integrated in lab-on-chip devices.[15] Following this strategy, domain structuring of ferroelectric surfaces[16–18] allows the use of the associated electrostatic fields and/or suitable electrochemical reactions for manipulation and patterning of molecules and nanoparticles.[19–21] Pyroelectric fields in domain structured ferroelectric surfaces have been also proposed to induce the dielectrophoretic (DEP) forces required for nanoparticle patterning.[22]

A few years ago, a new method based on the high electrostatic evanescent fields generated by visible illumination of the surface of certain photovoltaic (PV) crystals, mainly Fe:$LiNbO_3$, has been proposed for manipulation of cells and nano-objects. First tests of the method in the biomedical field for killing tumor cells in cancer therapy[23] have been demonstrated and their potential for trapping and patterning of nano-particles has been demonstrated.[24–27] The method, which has been designated as *photorefractive (PR) or photovoltaic tweezers*, relies on the electric fields generated under illumination in photorefractive crystals[28,29] mainly by the bulk photovoltaic effect.[30] The induced spatial electric field distribution is closely correlated with the light distribution. The corresponding evanescent fields extending outside the illuminated sample may act on either charged (*electrophoresis*) or neutral (*dielectrophoresis*) particles deposited on the sample surface. Theoretical formalisms to calculate the evanescent electric fields, mostly caused by the photovoltaic effect, and to discuss the performance of PV tweezers have been recently developed.[31,32] Reference 31 also includes a brief comparison with the performance of conventional optical tweezers. The main advantage of the new procedure is that the electrophoretic and dielectrophoretic forces associated to the PV electric fields do not require deposition of any electrodes and, moreover, parallel manipulation and flexible patterning of micro- and nano-objects can be achieved by using the imaging capabilities of light. Furthermore, the light-induced electric patterns can be erased thermally or by homogeneous illumination allowing for pattern reconfiguration and switching. In this sense, the PV method appears more convenient and flexible than those based on the capabilities of ferroelectric domain structuring.[33–35]

$LiNbO_3$ is a reference material[36] for electrooptic, nonlinear, photovoltaic, and photorefractive applications. A number of books are available on those subjects.[28–30,37] Specifically, for the trapping and patterning methods, discussed in this report, Fe:$LiNbO_3$ is, so far, the photovoltaic material presenting the highest PV electric fields (up to 2×10^5 V/cm, Refs. 30 and 38) along the polar *c*-axis. They are produced during illumination with a suitable light wavelength corresponding to optical transitions of the Fe^{2+} donor impurity. Other transition metal impurities, such as Cu and Mn, could also be used although the reported photovoltaic fields are somewhat lower.[34,39] Recently, high PV electric fields have also been observed in undoped congruent $LiNbO_3$ at high light intensities ($>100\,W/cm^2$) due to lattice defects (e.g., Nb antisites)[40–43] but they have been much less investigated. Moreover, to be exhaustive one should, here, mention a few papers that have also reported on a high PV current observed in undoped $LiNbO_3$ under X-ray excitation.[44–46] Although this effect might extend the capabilities of the method, there are only a few reports available and will not be further discussed in our present review. It is remarkable that in spite of the extensive effort devoted in the past to understand and exploit the PR and PV effects, their possible application to particle trapping and manipulation is very recent, although the reported results show a great technological potential.

The purpose of this work is to present a critical overview about the reported work on the use of light-induced photovoltaic evanescent fields in Fe:$LiNbO_3$ to induce trapping and patterning of nano-particles deposited on its surface. So far, the set of reported results on the method is still limited and many of its consequences and implications have not been explored and/or experimentally demonstrated. However, although the topic is still young, we feel that it is appropriate at this stage to present the capabilities of the method to stimulate new developments and applications. We start the review with Section II, devoted to describe the physical basis of the PV technique and proposed theoretical models, which provides a convenient scheme to deal with different aspects on the operation of PV tweezers. Section III describes different reported experimental configurations and procedures. In Section IV, we summarize the main experimental realizations on particle trapping and patterning. The role of different geometrical and physical parameters is stressed and the specific properties of the generated patterns are discussed. 1D and 2D patterns are considered separately. To complete the analysis in Section V other alternative methods using $LiNbO_3$, such as those based on UV illumination of periodic poling of the structure (PPLN)[35,47] or in the pyroelectric (PY) effect,[22,48,49] will be briefly discussed for comparison purposes. In Section VI, a variety of applications of PV tweezers that are mostly in a preliminary stage, are reviewed. Finally, Section VII stands out the promising capabilities of the trapping, manipulating, and patterning, of nanoparticles for useful devices in a number of technological areas.

II. PHYSICAL BASIS AND THEORETICAL DESCRIPTION

A. The bulk photovoltaic effect in $LiNbO_3$

The method for nano-particle manipulation to be discussed in the present review is based on the bulk PV effect occurring in $LiNbO_3$ as well as in other non-centrosymmetric dielectric crystals.[30,50] Therefore, it is appropriate to start with a brief summary of the PV effect for $LiNbO_3$, suitably doped with transition metal impurities, such as iron, which induces

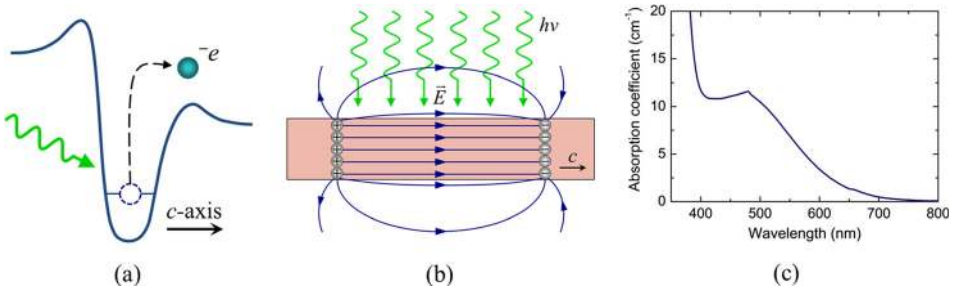

FIG. 1. (a) Diagram illustrating the PV mechanism. (b) Schematic representation showing the evanescent PV fields generated under light excitation. (c) Absorption spectrum for $LiNbO_3$:Fe.

the largest effect. Iron doping introduces two valence states, +2 and +3, whose concentrations keep a certain reduction ratio ($r = [Fe^{2+}]/[Fe^{3+}]$), depending on the total concentration and doping method. Visible illumination induces an asymmetric excitation of electrons[30] from the Fe^{2+} donor centers along the ferroelectric trigonal (poling) axis as it is schematically illustrated in Figure 1(a). This PV effect is a consequence of the non-centrosymmetric crystal lattice (point group 3m) around the absorbing iron atom. The directional electron excitation generates a photovoltaic current density j_{PV} that can be written as

$$j_{PV} = e\alpha l_{PV} I = esDl_{PV} I, \tag{1}$$

I being the light intensity (photon flux per unit time), α being the absorption coefficient, s being the photoinization cross section of donors, D being the donor concentration ($[Fe^{2+}]$), and l_{PV} being the PV drift length (~1–5 Å). The microscopic basis of the effect is the abrupt generation of an elementary electrical dipole moment, $p_{PV} = el_{PV}$, associated to the excitation of a Fe^{2+} donor center after absorption of one single photon. The PV asymmetrical photoionization is followed by charge migration and redistribution due to electron retrapping at acceptors Fe^{3+} centres. Under open circuit conditions, this charge transport process generates a correlated space-charge field, both, inside and outside (evanescent field) the sample, which is schematically drawn in Figure 1(b). The field inside the sample writes

$$E_{PV} = \frac{j_{PV}}{e\mu n}, \tag{2}$$

where μ is the electron mobility and n is the density of excited electrons that can be written as

$$n = \frac{sID}{\gamma A}, \tag{3}$$

A being the acceptor concentration ($[Fe^{3+}]$) and γ being the trapping coefficient of acceptors. Taken into account (1) and (3), expression (2) for the PV field becomes

$$E_{PV} = \frac{l_{PV} A}{\mu\gamma}. \tag{4}$$

Then, the magnitude of the field depends on the total iron concentration and the oxidation-reduction via the concentration of acceptor $[Fe^{3+}]$. This PV field modifies the refractive index of the material through the electrooptic effect (*photorefractive effect*). The high photovoltaic fields of Fe:$LiNbO_3$ seem to be related to its low electron mobility together with a high PV drift length for the iron impurities. The absorption spectrum of Fe^{2+}, which determines the efficiency of the PV effect (through the photoionization cross section s), covers the range from 350 to 600 nm and it has a peak at $\lambda = 480$ nm (see Figure 1(c)). Other impurities like Mn or Cu also show a (smaller) PV effect in a different spectral range.[39] The temporal dynamics (response time) depends on the light intensity, the electrical transport parameters, i.e., the electronic mobility, and the ratio $[Fe^{3+}]/[Fe^{2+}]$. More details about the PR effect can be consulted in suitable Refs. 30, 37, and 51.

B. Photovoltaic evanescent fields

PV tweezers operation is based in the action of light induced PV electric fields close to the crystal surface. Therefore, it is important to model these edge fields that we will call evanescent fields so far. It is worth to note that, although the theoretical description of the PV fields inside the crystal has been extensively addressed in connection with the photorefractive effect, little effort has been devoted to the evanescent fields. In Section II B 1, we will pay attention to the reported theory for sinusoidal illumination,[31,52] largely used in previous experiments, while the general case of arbitrary illumination patterns[53] will be dealt in Section II D.

1. Sinusoidal intensity profile and spatial harmonics of the PV field

Experiments performed under a periodic light intensity profile (*holographic experiments*) acting on the XY face (see Figure 2) of a slab sample, e.g.,

$$I = I_0(1 + m\cos Kx), \tag{5}$$

are well suited for quantitative analysis. Z is the normal to the slab, X is the PV (poling) axis that coincides with the trigonal crystallographic axis (c-axis) of $LiNbO_3$ and m $(0 < m < 1)$ is the modulation index or light contrast of the illumination pattern. In accordance with the standard photorefractive model that describes the build-up of the light-induced space charge, significant electric fields develop inside the sample and extend as evanescent fields into the surrounding medium. The problem of the charge transport giving rise to light induced electric fields in PR materials taken into account edge effects is not at all simple as described in a number of papers.[54,55] In addition, most formalisms neglect nonlinear contributions to charge transport what is only a good approach for low light contrast

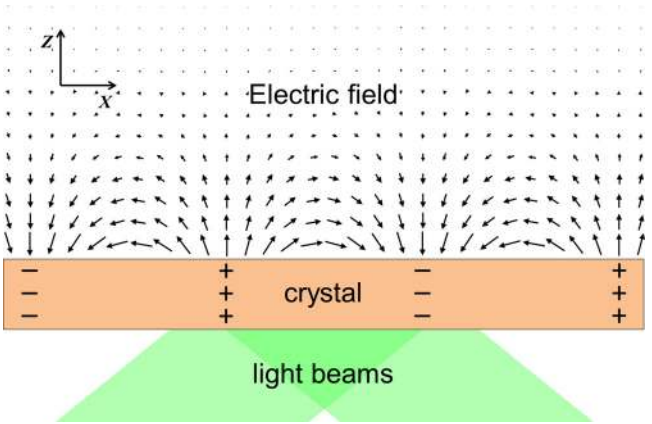

FIG. 2. Illustration of the evanescent photovoltaic electric fields E (represented by arrows) generated by a sinusoidal light pattern obtained by interference of two light beams.

conditions ($m \ll 1$) that is not convenient for particle trapping. We will present here the formalism developed in Refs. 31 and 52 for PV tweezers, which considers separately the cases of low light contrast and high light contrast m.

a. Low light modulation. For low m values, a linear approximation to carrier transport equations applies and sinusoidal space charge fields are developed inside the crystal. Then, under steady-state conditions, the field profiles inside the crystal ($z<0$) including edge effects (near the interface) write for the common case of dominant PV field

$$E_{X,in}(x,z) = -mE_{PV}\left(1 - e^{Kz}\frac{\varepsilon_m}{\varepsilon_m+\varepsilon}\right)\cos Kx, \tag{6a}$$

$$E_{Z,in}(x,z) = mE_{PV}\frac{\varepsilon_m}{\varepsilon_m+\varepsilon}e^{Kz}\sin Kx, \tag{6b}$$

where E_{PV} is the photovoltaic field and ε and ε_m are the static dielectric constants of the PV material and surrounding medium, respectively. Both field components linearly depend on the light modulation and they present a $\pi/2$ phase mismatch. The evanescent fields ($z>0$) are readily derived through the boundary conditions at the interface and write

$$E_{X,out}(x,z) = -mE_{PV}\frac{\varepsilon}{\varepsilon_m+\varepsilon}e^{-Kz}\cos Kx, \tag{7a}$$

$$E_{Z,out}(x,z) = mE_{PV}\frac{\varepsilon}{\varepsilon_m+\varepsilon}e^{-Kz}\sin Kx. \tag{7b}$$

Note that outside the crystal both components have the same modulus and decrease exponentially with the distance z to the crystal surface. Taking into account that for $LiNbO_3$, $\varepsilon = 30\varepsilon_0$ and for common values of the relative dielectric permittivity of the surrounding medium, not far from that of air, the magnitude of the evanescent PV field near the surface roughly equals the bulk PV fields. The field vectors near the surface of a PV crystal are illustrated in Figure 2.

b. High light modulation: Spatial harmonics of the PV field. In many experiments, light intensity profiles with high contrast (m close to 1) are used to achieve high electric fields and then, Eqs. (7a) and (7b) for the evanescent fields are no longer valid. One, then, has to take into account the nonlinearities of the charge transport equations describing the photorefractive response.[32,56,57] In this case, the space charge fields present harmonic contributions with K vectors that are multiple of the fundamental K of the light. The impact of this aspect on the PV tweezers has been also addressed in Refs. 31 and 52, considering an approximation that keeps the fundamental and the second harmonic components. The result indicates the importance of the presence of harmonics on the trapping and patterning processes. Up to second order in the harmonic expansion, the expressions for the evanescent fields become

$$E_{X,out}(x,z) = -E_K e^{-Kz}\cos Kx - E_{2K}e^{-2Kz}\cos 2Kx + \cdots, \tag{8a}$$

$$E_{Z,out}(x,z) = E_K e^{-Kz}\sin Kx + E_{2K}e^{-2Kz}\sin 2Kx + \cdots, \tag{8b}$$

where the evanescent fundamental and second harmonic amplitudes have the same relation with the corresponding bulk components as in Eqs. (6) and (7).

C. Photovoltaic tweezers: Forces on particles

The PV evanescent fields induce electrical forces on either the particles that are electrically charged (electrophoretic forces $\vec{f}_{ep} = q\vec{E}$) or those neutral that become polarized by the field (dielectrophoretic forces). These forces allow the manipulation and trapping of micro and nano-objects providing a new kind of optoelectronic tweezers, which is frequently designated as photovoltaic tweezers. Most work has been performed on dielectrophoretic forces that require a more elaborated analysis described below.

1. DEP forces

The DEP force acting on a neutral dielectric particle placed close to the sample surface is

$$\vec{f} = -\vec{\nabla}(-\vec{p}\cdot\vec{E}), \tag{9}$$

$\vec{p}$ being the dipolar momentum of the particle induced by the evanescent field $\vec{E}$. Due to the crystalline and/or geometrical anisotropy of particles, the dipolar momentum induced by the electric field obeys, in general, a tensor expression

$$p_i = \varepsilon_0\alpha_{ij}E_j, \tag{10}$$

α_{ij} being the second order polarizability tensor of the particle and ε_0 being the vacuum permittivity.

In the very relevant case of spherical and crystallographically isotropic particles and assuming the Rayleigh approximation (particle radius $R \ll \Lambda = 2\pi/K$), the polarizability becomes a scalar α_p and writes[31]

$$\alpha_p = 6V\varepsilon_m\frac{\varepsilon_p-\varepsilon_m}{\varepsilon_p+2\varepsilon_m}, \tag{11}$$

$V = 4\pi R^3/3$ being the volume of the particle and ε_m and ε_p being the relative dielectric permittivities of the host medium

(often air) and particle, respectively. For highly conductive particles (e.g., metals) $|\varepsilon_p| \gg \varepsilon_m$, the above equation leads to

$$\alpha_p = 6V\varepsilon_m. \tag{12}$$

One should put some caution on these expressions, (11) and (12), since the close presence of the substrate material may impose some small anisotropy on the polarizability α_p.[58]

For this isotropic case:

$$\vec{f} = -\vec{\nabla}U = -\vec{\nabla}(-\varepsilon_0\alpha_p E^2), \tag{13}$$

$U = -\varepsilon_0\alpha_p E^2$ being the DEP potential energy.

Using expression (13) with expressions (8a) and (8b) for the evanescent fields, one obtains for the components of the force perpendicular f_Z and parallel f_X to the crystal substrate

$$f_Z = -\varepsilon_0 K 2\alpha_p E_K^2\left[e^{-2Kz} + 3\frac{E_{2K}}{E_K}e^{-3Kz}\cos Kx\right], \tag{14a}$$

$$f_X = -\varepsilon_0 K 2\alpha_p E_K{}^2\frac{E_{2K}}{E_K}e^{-3Kz}\sin Kx. \tag{14b}$$

Both components increase linearly with K. The parallel component f_X has only one sinusoidal term with the same period of light K, which linearly depends on $\delta = E_{2K}/E_K$. On the other hand, the vertical component f_Z has also a sinusoidal term linearly dependent on δ but $\pi/2$-shifted with regard to f_X, and a homogeneous term independent of δ. It is interesting to highlight that for low modulation ($m < 0.2$), $\delta \approx 0$ and only the homogeneous vertical (attractive) term remains, leading to spatially homogeneous trapping. Then, the use of low m values provides a procedure to obtain homogeneous particle trapping on the substrate. For higher modulation, i.e., for a non-negligible δ, the two components have sinusoidal terms that give rise to periodic particle patterns with the same periodicity of the exciting light. Moreover, Eq. (14a) for f_Z implies that for high enough δ, the illuminated pattern presents alternative regions with repulsive ($f_Z > 0$) and attractive forces ($f_Z < 0$), as illustrated in Figure 3. There, the normalized vertical force component f_Z/f_0 ($f_0 = \varepsilon_0 K 2\alpha_p E_K^2$) as a function of the spatial coordinate x is plotted for three δ values, 0.2 (blue dotted line), 1/3 (black dashed line), and 0.4 (red solid line). The value $\delta = 1/3$ is a threshold that separates two different regimes. For $\delta < 1/3$, the homogeneous term in expression (14a) dominates and so the vertical component is attractive (i.e., $f_Z/f_0 < 0$) throughout the whole period. For $\delta > 1/3$, the sinusoidal term is the largest one and consequently there is a region in the middle of the period for which the force on particles is repulsive (as indicated by the arrows in Figure 3). Consequently, one can conclude that the value of δ, controlled by the light modulation, is a key parameter to optimize the contrast of the patterns.

Finally, it is worthwhile remarking that the two f_X and f_Z components decay exponentially with the distance z as clearly seen in Eqs. (14a) and (14b). For the sinusoidal terms, the decay constant is $3K$ and for the homogeneous term is $2K$. On should note that the decays are faster for the DEP forces than for the electrophoretic ones whose decay constant is K.

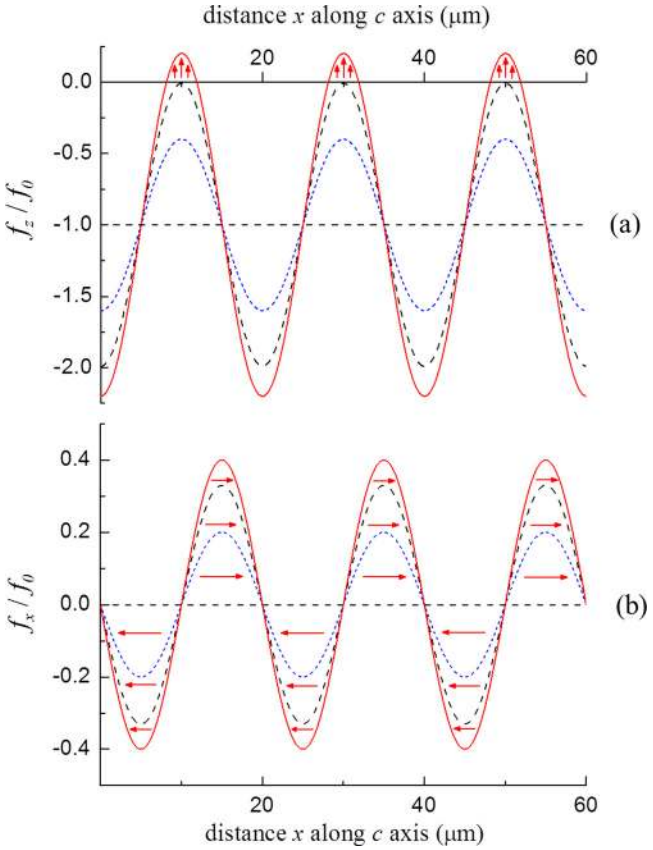

FIG. 3. (a) Normalized vertical f_Z/f_0 and (b) horizontal f_X/f_0 force components as a function of the spatial coordinate x along the c-axis for exposure to a sinusoidal light pattern and three different values of $\delta = E_{2K}/E_K$: 0.2 (blue dotted line), $1/3 = 0.33$ (black dashed line), and 0.4 (red solid line). The arrows indicate (a) the region of repulsive f_Z and (b) the direction of f_X in each region. Reprinted with permission from Matarrubia *et al.*, J. Phys. D **47**, 265101 (2014). Copyright 2014 Institute of Physics.

In many cases, one uses particles having crystallographic (structural) anisotropy or non-isotropic shapes (geometrical anisotropy) making the effective polarizability α_{ij} a second-order tensor. Generally, the later type is the most common source of anisotropy. Many smooth shapes can be approximately represented by an ellipsoid having three principal axes and different polarizabilities along them. When the particles are attracted to the surface of a PV sample the DEP forces acting on them would depend on the relative orientation of their axes (u, v, w) versus the macroscopic axes X, Y, Z of the experiment (see Figure 4) and can be calculated through the more general formula

$$f_l = \varepsilon_0\nabla_l(\alpha_{ij}E_jE_i), \quad l,i,j = 1,2,3. \tag{15}$$

A main effect of these forces is to align the particle axes along the macroscopic axes of the experiment. A simple case for analysis corresponds to the particles that present a rotational symmetry axis. For example, for disk-shaped particles[37] deposited on the surface, having its u, v axes in the disk plane coinciding with the X, Y axes of the substrate. The tensor components of the polarizability write

$$\alpha_{xx} = \alpha_{yy} = V(\varepsilon_p - \varepsilon_m), \tag{16a}$$

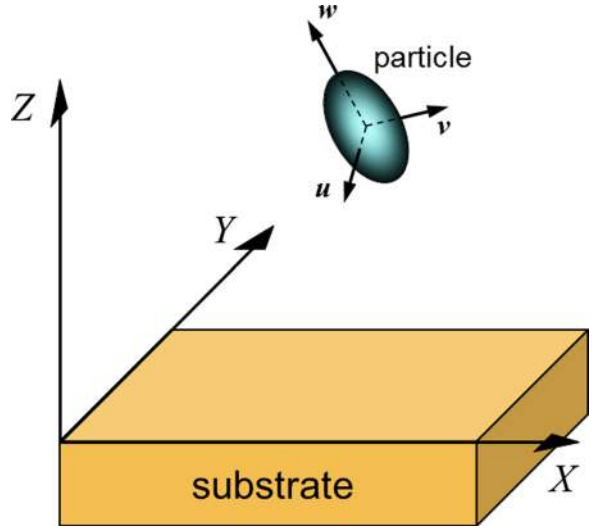

FIG. 4. Schematic representation showing the axes of an anisotropic particle.

$$\alpha_{zz} = V\varepsilon_m \frac{\varepsilon_p - \varepsilon_m}{\varepsilon_p}. \tag{16b}$$

On the other hand, for rod-shaped particles, taking Z along the cylindrical axis

$$\alpha_{xx} = \alpha_{yy} = 2V\varepsilon_m \frac{\varepsilon_p - \varepsilon_m}{\varepsilon_p + \varepsilon_m}, \tag{17a}$$

$$\alpha_{zz} = V(\varepsilon_p - \varepsilon_m). \tag{17b}$$

Let us focus for simplicity on the structure of DEP forces acting on disk-shaped particles. Assuming that all particles have their principal axes oriented along the axes (*X*,*Y*,*Z*) of the experimental configuration (see Figure 2), the corresponding DEP forces, Eq. (12), become up to the second harmonic in the field profile

$$\begin{aligned} f_Z = &-\varepsilon_0 K E_K^2 e^{-2Kz}[(\alpha_{XX} + \alpha_{ZZ}) + 2(\alpha_{XX} - \alpha_{ZZ})\cos 2Kx] \\ &-3\varepsilon_0 K E_K^2 \delta\, e^{-3Kz}[(\alpha_{XX} + \alpha_{ZZ})\cos Kx \\ &+ (\alpha_{XX} - \alpha_{ZZ})\cos 3Kx], \end{aligned} \tag{18a}$$

$$\begin{aligned} f_X = &\varepsilon_0 K E_K^2 e^{-2Kz}(\alpha_{XX} - \alpha_{ZZ})\sin 2Kx \\ &-\varepsilon_0 K E_K^2 \delta\, e^{-3Kz}[(\alpha_{XX} + \alpha_{ZZ})\sin Kx \\ &+ 3(\alpha_{XX} - \alpha_{ZZ})\sin 3Kx]. \end{aligned} \tag{18b}$$

In this case, the expressions have more harmonic terms whose relative importance depends on particle anisotropy through (α_{XX}-α_{ZZ}) and on the light modulation via $\delta = E_{2K}/E_K$. It is important to remark that in this case at low *m* (i.e., negligible δ) there is still particle structuring with a periodicity $\Lambda/2$ at difference with the isotropic case.

In summary, the theoretical model predicts a key role of higher harmonics (via $\delta = E_{2K}/E_K$) what will be confirmed when discussing experiments. Depending on volume and permittivity of the deposited particles, DEP forces can easily reach values well above gravity forces (up to a factor $\sim 10^3$). For example, they are around 10 pN for particles having a volume $V = 1\,\mu m^3$ and lying at a high field grating region (50 kV/cm).

On the other hand, the expressions for the polarizabilities (Eqs. (10), (15), and (16)) offer a clear indication of the competing role of the particle dielectric constants and the surrounding medium. In particular, if they are equal the DEP forces extinguish.

D. Arbitrary intensity profiles

The theoretical description of Sections II A–II C is restricted to sinusoidal illumination and considers only the fundamental and second order harmonic terms, neglecting higher order components of the PV fields. However, the PV tweezers can use 2D arbitrary light intensity patterns and a more general approach is necessary to accurately describe particle patterning. To this end, Arregui *et al.*[53] have developed a numerical tool to analyze the EP and DEP particle trapping for arbitrary light patterns avoiding the previous assumptions. It is based on an iterative finite differences algorithm that calculates all the relevant magnitudes in two steps: (i) first, the space charge field inside the crystal is calculated and (ii) second, the corresponding evanescent fields and the DEP potential are obtained. Particles should trap in the minima of this potential so that from it one can inferred the main features of the particle patterns. Note that the main restriction of this formalism is that the calculated the DEP potential is only valid for isotropic particles. The algorithm is applied to a number of 1D and 2D light patterns including sinusoidal and Fresnel lens-type illumination, a Gaussian beam, and the interference of two Gaussian beams. The theoretical predictions are compared with appropriate experiments showing very good overall agreement. Moreover, the results derived from that rigorous formalism, for sinusoidal illumination at low and high light modulation, coincide with the prediction of Section II C obtained with the simple analytical model giving a further support to its applicability.

E. Final remarks on the theoretical formalism

There are a number of aspects of the problem that have been, so far, ignored in the current theory for PV particle trapping. First, all theoretical results correspond to the stationary situation and it does not consider the dynamics of the process. In addition, the model describes the PV tweezers operation when the polar axis of the substrate and then the PV field are parallel to the crystal surface (*x*- and *y*-cut substrates). This is the ordinary situation in previous works that we will call parallel configuration. However, very recently, a new geometry, with the polar axis normal to the surface (i.e., using *z*-cut substrates), has been used. A first theoretical formulation has been already reported[59] for this geometry, which we will call perpendicular configuration.

Another aspect to consider has to do with the particular deposition method and the nature of the depositing (surrounding) medium. In particular, other forces acting on the process such as adhesion forces to the substrate and forces among particles (that may be comparable with the DEP forces) and Brownian motion (particularly in the case of liquids) have not been considered. In fact, the PV tweezers operation includes two physical processes, PV field build-up and particle deposition, which can be either sequential or

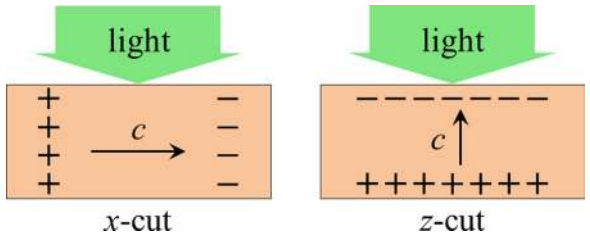

FIG. 5. Schematic representation of the parallel and perpendicular configurations showing the distribution of charges inside the crystal under homogeneous illumination of its surface.

simultaneous. In the former case, the dynamics of particles can influence the PV field build-up. In the sequential case, dealing with low light intensities, buoyancy, and Marangoni forces that have been shown to be relevant in optical tweezers is not expected to be significant. Anyhow, all those points should deserve further attention in future work and would require new specific experiments that could be very relevant in some of the prospective applications to be discussed in Sections IV D and V, particularly in relation to particle dragging and pattern reconfiguration.

III. EXPERIMENTAL PROCEDURES

The operation of PV tweezers involves the deposition and ordered arrangement of micro and nano-objects on photovoltaic substrates illuminated by visible light patterns. Let us review separately the different experimental aspects of the process.

A. Photovoltaic substrates

In most cases, the PV substrates are *x*- or *y*-cut Fe:$LiNbO_3$ plates containing the photovoltaic *c*-axis. The total iron doping is high, in the 100–1000 ppm range, to obtain high PV fields (10–100 kV/cm). In turn, the oxidation/reduction state of the substrate, i.e., the ratio ($r = [Fe^{3+}]/[Fe^{2+}]$), strongly influences the PV response because the time constant τ for the build-up of the PV fields is proportional to *r*. For example, Esseling *et al.*[60] have modified the oxidation-reduction state *r* obtaining a decrease of the τ value of about one order of magnitude (a few seconds for relatively low intensities of 200 mW/cm^2). In addition to the standard *x*- and *y*-cut plates (parallel configuration), the *z*-cut substrates (perpendicular configuration) have also been very recently used. The two configurations, parallel and perpendicular, are schematically drawn in Figure 5.

Although samples of Fe-doped $LiNbO_3$ are the most used for PV particle trapping, other types of $LiNbO_3$ substrates, even undoped crystals relying on Nb_{Li} intrinsic defects[40–43] may be the useful options for future work. Another novel approach recently reported[61] is the use of Fe:$LiNbO_3$ optical waveguides as substrates for the PV tweezers operation. Specifically, the particle trapping has been demonstrated for two types of Fe:$LiNbO_3$ planar waveguides, proton-exchanged[62] and swift-heavy ion irradiation[63] guides. Apart from $LiNbO_3$, another photorefractive crystal, BSO ($Bi_{12}SiO_{20}$), has also been successfully used as substrate for light-induced particle trapping.[64] This material does not have a photovoltaic effect as $LiNbO_3$, and it is necessary to apply an external electric field to produce the separation of photo-induced charges. The main advantage of using this crystal is the faster time response (at least one order of magnitude shorter than the fastest reported experiments with Fe:$LiNbO_3$), although the obtained patterns are less defined than those obtained in that crystal.

B. Illumination schemes

In order to induce PV fields different types of illumination set-ups have been used in the experiments reported so far. The first and simplest one consists of illuminating the material with a single beam either directly or through a mask. Illumination with incoherent sun light has been also reported.[52] More often, experiments use a holographic configuration. The typical set-up is schematically illustrated in Figure 6. The light sources used were He-Ne (633 nm), Ar-ion (488 nm), or frequency-doubled Nd:YAG (532 nm) lasers with typical intensities in the range of 1–100 mW/cm^2. The lasers beams are expanded to achieve a homogeneous interference pattern. This holographic configuration allows creating sinusoidal periodic light patterns with periods ranging from a few hundred nanometers to hundreds of micrometers.

A third illumination scheme for the generation of PV electric fields, first utilized by Esseling *et al.*,[27] involves the projection of an image generated by a spatial light modulator (SLM). This lighting system is very useful to handle arbitrary 2D light patterns. Finally, as previously mentioned, guided light has been also used in some experiments.[61] The illumination pattern is generated by interference of two laser beams coupled into the waveguide through a rutile prism (see Figure 7). Waveguides offer an additional advantage since light confinement at the micrometer scale allows for

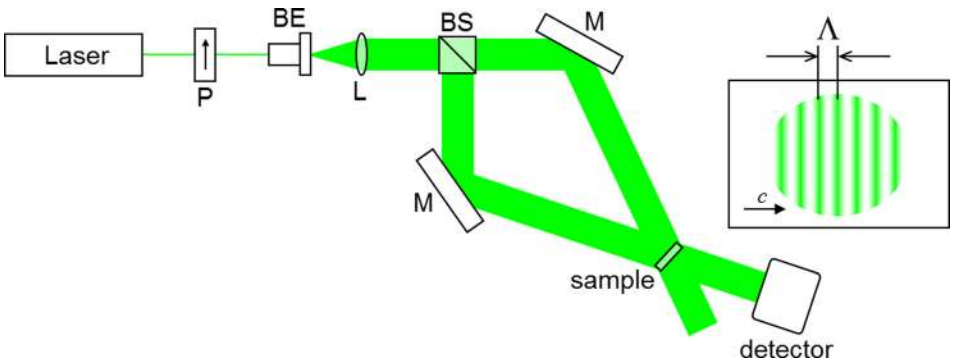

FIG. 6. Experimental setup for holographic illumination. P polarizer, BE beam expander, L lens, BS beam splitter, and M mirrors. Reprinted with permission from Burgos *et al.*, Opt. Mater. **35**, 1700 (2013). Copyright 2013 Elsevier.

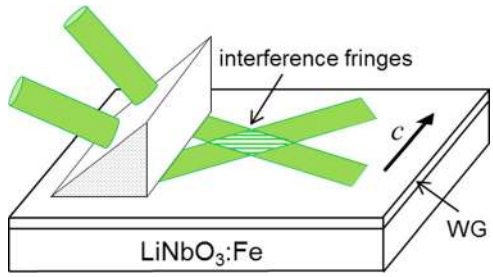

FIG. 7. Experimental setup for holographic illumination through an optical waveguide to allow for particle deposition on its surface. Reprinted with permission from Jubera *et al.*, Opt. Lett. **39**, 649 (2014). Copyright 2014 Optical Society of American.

high light intensities ($\sim$kW/cm^2) and so, shorter PV response times.

C. Particles and deposition methods

A variety of micro and nanoparticles, either commercially available or prepared by crushing or chemical methods, have been used in reported experiments. They include dielectric materials as polystyrene,[24] chalk ($CaCO_3$),[25,31] silicon carbide,[25] semimetals as graphite,[27,52] and metals such as aluminium and silver.[26,65] Anisotropic (graphite and $CaCO_3$) as well as isotropic spherical particles (polystyrene, Ag, and Al) have been used. The particles had linear dimensions or diameters ranging from $\sim 1\,\mu$m ($CaCO_3$, graphite, and polystyrene) to 70–80 nm (Ag and Al). Prior to particle deposition, the $LiNbO_3$ samples might be coated with an antireflection coating,[25] although in most cases the surface is not subjected to any physical or chemical treatment.

A relevant issue, not sufficiently understood, is the role of the host medium where particles are embedded and the deposition method. A schematic representation of the different reported methods is shown in Figure 8. Particles have been deposited not only in air[25,52] or from a liquid suspension, mostly organic (hexane and tetradecane),[26,27,65] but also from an aqueous solution.[24,66,67] When using deposition in air, two possibilities has been reported: the particles are sprayed on the sample (Figure 8(a)) or they are deposited homogeneously on the sample and, then, they are blown from the top to remove those ones that are not firmly attached to the surface (Figure 8(b)). In the case of using a liquid suspension of particles, either a drop is deposited on the surface (Figure 8(c)) or the whole substrate is introduced in the liquid (Figure 8(d)). Illumination and deposition of the particles can be done either simultaneously or sequentially and in both cases particle structuring has been achieved. The sequential method is experimentally simpler but for real time manipulation simultaneous operation is obviously necessary.

IV. EXPERIMENTAL RESULTS ON TRAPPING AND PATTERNING

Most experiments have been performed using the parallel configuration (substrate polar axis parallel to the surface), except those of Section IV C 1 that is devoted to a few recent results performed under the perpendicular configuration. Next, we will describe the main experimental results classified according to the used illumination scheme.

A. Single beam experiments

The reported results using single beam illumination,[31,52,67] namely, a Gaussian laser beam or an homogenous beam (expanded laser beam or sun light), through a rectangular mask, have provided a first qualitative insight into the physics of trapping. Figure 9 shows illustrative results of the trapping pattern obtained with $CaCO_3$ microparticles and the light illumination patterns mentioned above. In all cases, the deposited particles concentrate on the extremes of the illuminated region where the charges excited by light become accumulated. The clear symmetric particle pattern observed is an indication that the DEP forces are acting on neutral particles. For uniformly charged particles, one would expect that they should concentrate only in one of the two boundaries depending on the sign of the charges. In other words, this illumination configuration is useful to distinguish between the DEP forces acting on neutral particles and the EP forces that act on charged particles.

Finally, some experiments use one beam illuminating a binary stripe pattern as reported in Refs. 25 and 64.

B. Holographic configuration for one-dimensional patterning

The first experiments of particle trapping and patterning using photovoltaic fields in $LiNbO_3$ were made illuminating with light fringes obtained by the interference of two laser beams (holographic configuration).[24,25] This illumination has been often used because its suitability to obtain 1D periodic patterning. In addition, it is particularly appropriate to investigate the influence of the different experimental parameters in connection with the theoretical model.

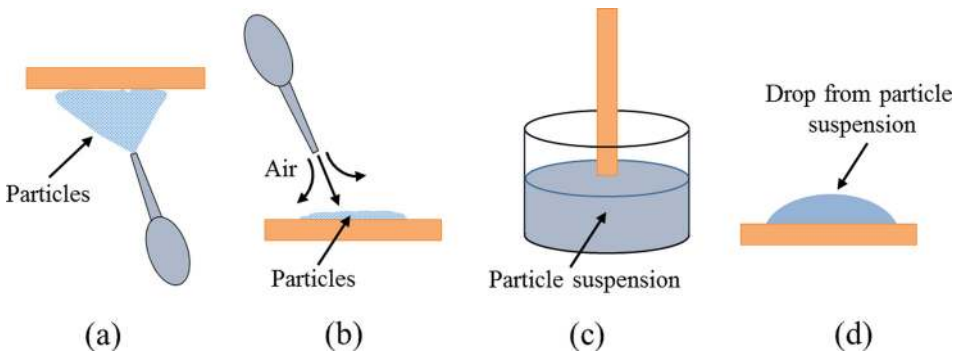

FIG. 8. Illustration of the particle deposition methods in air ((a) and (b)) and using a liquid suspension ((c) and (d)) (see text).

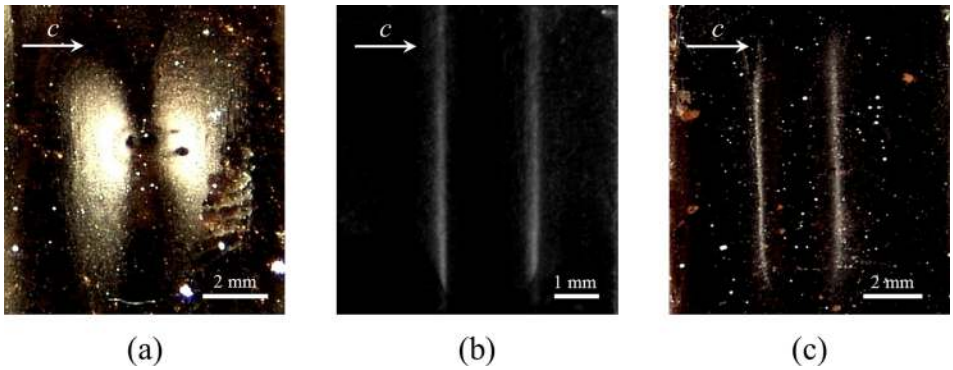

FIG. 9. Photograph of the patterns obtained with $CaCO_3$ microparticles under single beam illumination: (a) Gaussian laser beam ($\lambda = 532$ nm). (b) Expanded Gaussian laser beam and (c) homogeneous beam of sun light, passing through a rectangular slit. (a) and (c) Reprinted with permission from Burgos *et al.*, Opt. Mater. **35**, 1700 (2013). Copyright 2013 Elsevier. (b) Reprinted with permission from Muñoz-Martínez *et al.*, Opt. Mater. Express **5**, 1137 (2015). Copyright 2015 Optical Society of American.

Figure 10 shows a representative result under sinusoidal illumination with a period $\Lambda = 220\,\mu$m taken from Ref. 25. The particles were deposited on the surface and after PV recording the particles not attached were blown away. The fringes of chalk particles can be clearly seen and show a spatial period that is double than that of the light pattern. However, in the experiment by Sarkisov *et al.*[24] using polystyrene microspheres, the light and particles patterns present the same periodicity ($\Lambda = 12\,\mu$m). Other reported results reproduce this discrepancy obtaining either double[64] or the same periodicity of sinusoidal light excitation.[31,67] This issue, which is relevant because it has implications regarding the fidelity of the technique replicating the light pattern, has been analysed in Refs. 52 and 68. Taking into account the theoretical framework exposed in Section II, the authors provide an explanation to those experimental results as a consequence of the isotropy/anisotropy of the particles and the deposition method. If the particles are first homogenously distributed on the substrate and then blown away, only those anchored by the vertical trapping forces remain on the surface, and constitute the final observed pattern (2Λ spatial period). However, when the particles are deposited by spraying in air beneath of exposed surface, the evanescent fields may act time enough to align the particles along them and, consequently, they behave as isotropic particles. When using deposition from a liquid suspension the actual situation may be intermediate, and some particles are expected to be aligned along the field together with particles without any preferred orientation. Experiments showing these effects have been reported in those works and illustrated in Figure 11, where graphite micro-flakes and high light modulation is used. The periodicity of the particle pattern is clearly the same as that of the light for particles sprayed in air (Figure 11(a)), whereas one observes half the period of the light for particles that have been blown away after direct homogeneous deposition (Figure 11(b)). For particles suspended in a liquid solution (see Figure 11(c)), the situation appears analogous to that for the first case. However, the mean free path between collisions is much shorter in the liquid than in the air and so the alignment effect may be less effective.

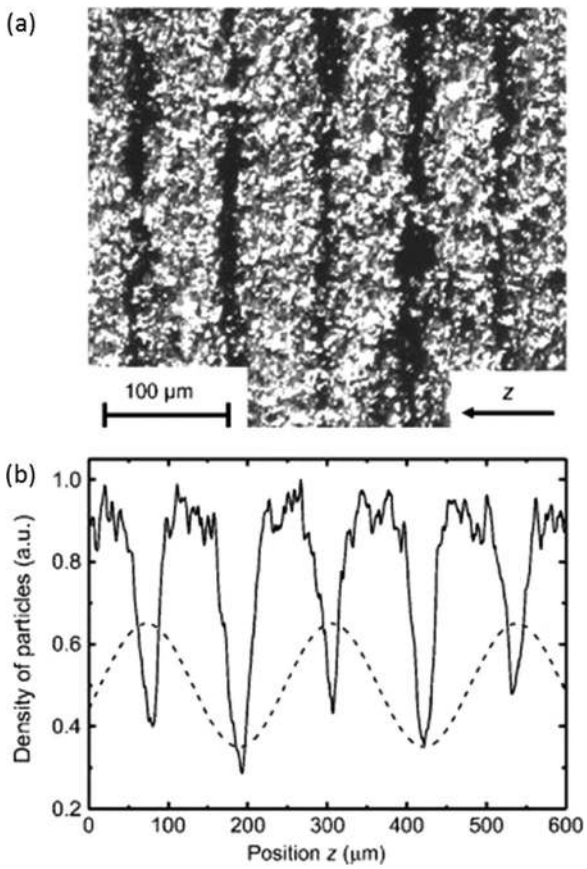

FIG. 10. (a) Photograph showing fringes of chalk particles trapping on $LiNbO_3$:Fe after sinusoidal illumination. (b) Relative density of particles (solid line) has been drawn together the light amplitude pattern used (dashed line). Reprinted with permission from Appl. Phys. Lett. **90**, 241909 (2007). Copyright 2007 AIP Publishing LLC.

Finally, it is worth to mention that holographic experiments have also been performed by coupling the two interference beams in a Fe:$LiNbO_3$ waveguide[61] using the experimental setup schematically shown in Figure 7. Good patterns with the same periodicity of light have been obtained for spherical aluminum nanoparticles with an illumination time as short as 3 s using $I = 700\,\text{W/cm}^2$. This configuration may be particularly useful in microfluidics and for combination with integrated optical devices (see Section VI).

1. Role of the light modulation and particle anisotropy

The theoretical model predicts a key role of the modulation index m of the exciting light in the trapping and patterning process that is cross correlated with particle anisotropy (see Section II). A recent detailed work[65] has corroborated this prediction using holographic experiments with spherical isotropic (Al and Ag) particles, and anisotropic flake-shaped (graphite) particles. Main experimental results are resumed in Figure 12.

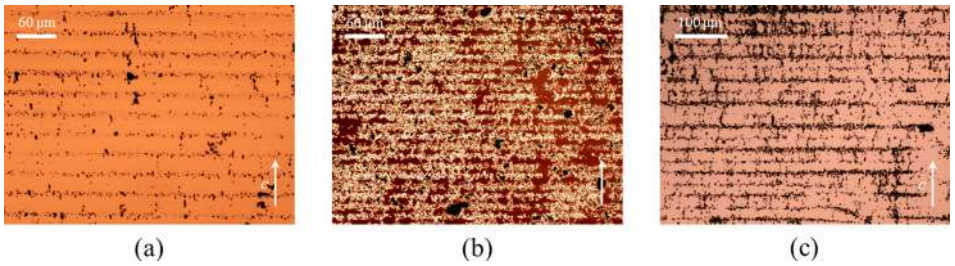

FIG. 11. Patterns obtained with graphite microparticles using different deposition methods. (a) Particles sprayed in air beneath the exposed surface. (b) Particles homogenously deposited on the surface and, subsequently, blown away. (c) The substrate is immersed in a hexane suspension of the particles. For (a) and (b), the spatial period of light distribution was 30 μm, while for (c) was 50 μm. In all cases, the light contrast is $m \sim 1$. Reprinted with permission from Burgos *et al*., Opt. Mater. **35**, 1700 (2013). Copyright 2013 Elsevier.

According to the theoretical description, for isotropic particles (Al) and high light modulation ($m \sim 0.9$) well defined patterns having the periodicity of the light have been recorded, as it is shown in Figure 12(c). On the other hand, in the case of low index modulation ($m = 0.2$), there is no observable patterning, as clearly seen in Figure 12(a), but only homogeneous trapping because only the homogeneous and attractive vertical force component is non-negligible (i.e., $E_{2K} \approx 0$ in Eq. (14a)). The existence of PV homogeneous trapping is, indeed, confirmed from a comparison with a reference experiment in the absence of illumination (inset in Figure 12(a)). An intermediate situation is recorded for a value $m = 0.5$ (Figure 12(b)).

For anisotropic particles, the two DEP force components (longitudinal and vertical to the surface) present one structuring term grating vector $2K$ (i.e., $\Lambda/2$ spatial periodicity). Resulting patterns are illustrated for anisotropic graphite particles using a light grating period of 55 μm and indexes modulation $m = 0.5$ and $m = 0.9$ (Figures 12(d) and 12(e), respectively). The $2K$ structuring term can be distinguished, specially, in Figure 12(e).

2. Role of light period: Spatial resolution

So far, most experiments have used light grating periods of 100–500 μm (Refs. 25–27 and 69) for the light excitation, although much smaller gratings should be achievable, particularly, in reflection holographic configurations for which the smaller light period is $\sim\Lambda/2$, i.e., about 200 nm. It is clear that particles of small size, in the nanometric range, must be used to get patterning with those very short periods, since the relevant parameter to characterize the longitudinal resolution of the pattern is d/Λ. In fact, the requirements on the size of the particle are, even, tougher because the vertical decay range of patterning DEP forces falls rapidly with the distance z to the surface as $\exp(-3z/\Lambda)$ (see Eq. (14)) so that the total trapping force on the particle becomes strongly reduced when its diameter is comparable to Λ. Taking into account these theoretical aspects and then using small particles of nanometric size ($d \sim 70$ nm), much smaller particle pattern periods up to 4 μm have been recently reported (see Figure 13).[65] In fact, with further optimization, submicrometer periods could be very likely obtained.

3. Electrophoretic 1D patterns

While the PV DEP trapping has been largely investigated as described so far in this review, works reporting 1D electrophoretic trapping of charged particles are very scarce, probably because the range of applications with neutral

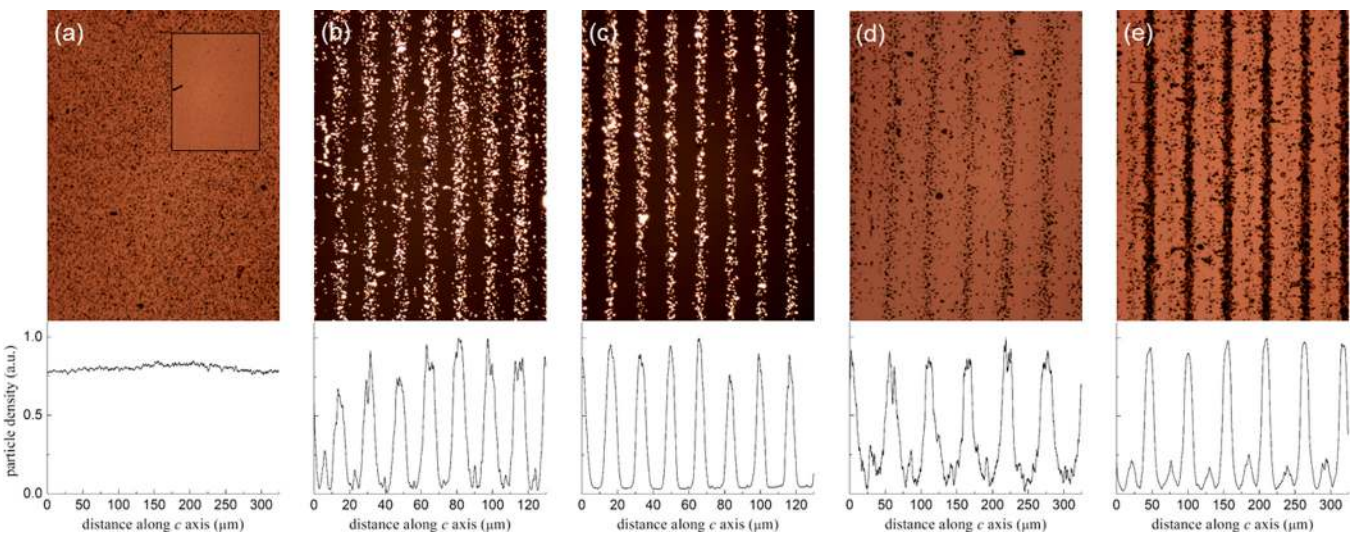

FIG. 12. Particle patterns obtained under sinusoidal illumination for Al ((a)–(c)) and graphite ((d) and (e)) and different light modulations (a) $m = 0.2$, (b) (d) $m = 0.5$, and (c) and (e) $m = 0.9$. The light periods are 18 and 55 μm for Al and graphite patterns, respectively. The inset of (a) shows a control experiment without illumination (see text). At the bottom of each image, the corresponding averaged particle concentration profile along the c-axis direction is shown. Reprinted with permission from Matarrubia *et al*., J. Phys. D **47**, 265101 (2014). Copyright 2014 Institute of Physics.

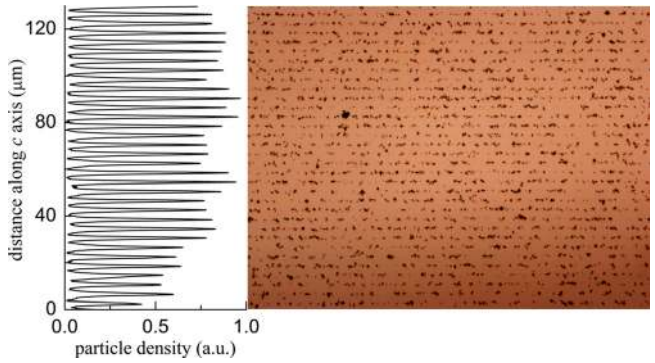

FIG. 13. Optical microscope image of a pattern with Al particles ($d \sim 70$ nm) and a spatial periodicity $\Lambda = 4.2\,\mu$m that coincides with that one for the light pattern. The light modulation is $m = 0.9$. Reprinted with permission from Matarrubia *et al.*, J. Phys. D **47**, 265101 (2014). Copyright 2014 Institute of Physics.

particles is larger. In Ref. 26, first successful experiments under sinusoidal illumination with charged micrometric particles are reported. On the one hand, they carried out experiments with only positively charged Al particles that structure with the same periodicity Λ of light (Figure 14(a)). On the other hand, they simultaneously used both, positive (Al) and negative (carbon particles), which trap at different places, separated by $\Lambda/2$, as expected for charges of opposite signs (Figure 14(b)). Besides, there are additional works reporting 2D periodic patterning of charged particles that will be cited in Section IV C.

C. Two-dimensional patterning

A key technological aspect for the practical application of PV tweezers is the capability to obtain high quality and flexible two-dimensional patterning. Esseling *et al.*[27] reported first experimental demonstrations on two dimensional DEP trapping of graphite particles using a spatial light modulator and laser light. However, the usual parallel experimental configuration presents serious limitations for such DEP patterning due to the preferential direction of PV charge transport along the polar axis parallel to the surface. As a consequence, particle fringes parallel to this axis are not allowed and the particles are trapped only at the boundaries of the illuminated regions. These effects distort the particle patterns that disappear at certain directions and are not a replica of the light distribution, as shown in Ref. 52 for a Fresnel-lens type illumination and in Ref. 27 for a mosaic of solid triangles. In this latter case (see Figure 15), the graphite particles are trapped preferentially perpendicularly to the *c*-axis at the edges of the triangles that are not sharply defined. Elimination of this drawback is very important for the development of PV tweezers and has been very recently addressed using a new configuration, the perpendicular configuration (already shown in Figure 5). The results are described in Section IV C 1. Alternatively, one can use 2D electrophoretic (EP) trapping of charged particles. This has been attempted by Esseling *et al.*[64] in a BSO crystal still using a parallel configuration but applying an AC bias field. They illuminated the crystal with a square pattern and obtained 2D structuring with a discrete definition very likely due to the lower photorefractive fields generated in this non photovoltaic crystal.

1. Perpendicular configuration

The proposed perpendicular configuration uses Z-cut substrates with the polar axis normal to the surface so that the PV effect occurs mainly along this direction. A simple schema to illustrate the bulk charge distributions generated under homogeneous illumination for both, parallel and perpendicular, was illustrated previously in Figure 5. Note that the perpendicular configuration is advantageous with regard to the parallel one since all direction in the substrate surface plane are equivalent for DEP as well as EP forces. A remarkable contribution using this latter configuration to trap charged particles (i.e., using electrophoretic forces) has been recently published.[70] Arbitrary 2D patterns have been obtained with good quality, overcoming the limitations of the parallel configuration used so far. An example of these patterns is shown in Figure 16.

In addition, successful experiments of 2D PV patterning in this perpendicular configuration but with DEP forces acting on neutral particles have been also very recently reported.[59,71] 2D particle patterns that are good replicas of the corresponding light patterns are also obtained.

We believe that the perpendicular configuration is an outstanding advance in the development of PV tweezers assuring high quality 2D patterning of charged and neutral particles and much simpler light control of the trapping regions. This implies a remarkable progress that could convert PV tweezers in a very competitive tool among optoelectronic particle trapping techniques.

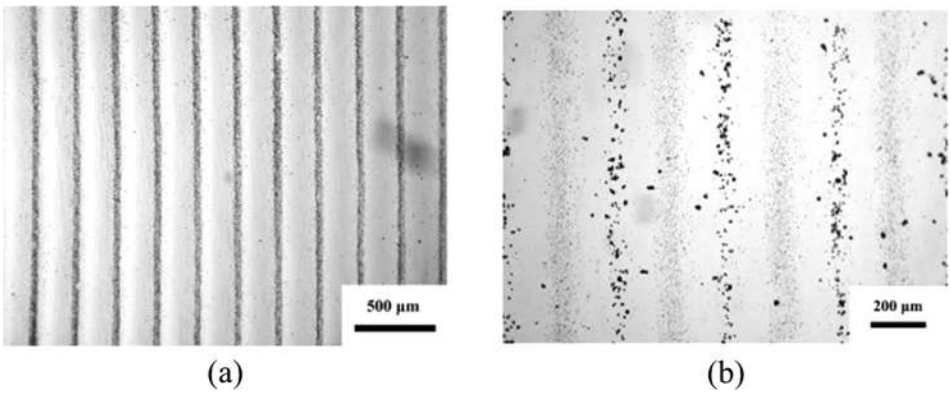

FIG. 14. (a) Particle pattern of positively charged aluminum particles with the same period of light ($\Lambda = 250\,\mu$m). (b) Patterns of negatively charged carbon (black) and positively charge aluminum (gray) particles aligned alternatively. The period of each particle grating was $400\,\mu$m coinciding with the period of sinusoidal illumination. Reprinted with permission from Zhang *et al.*, Opt. Express **17**, 9981 (2009). Copyright 2009 Optical Society of American.

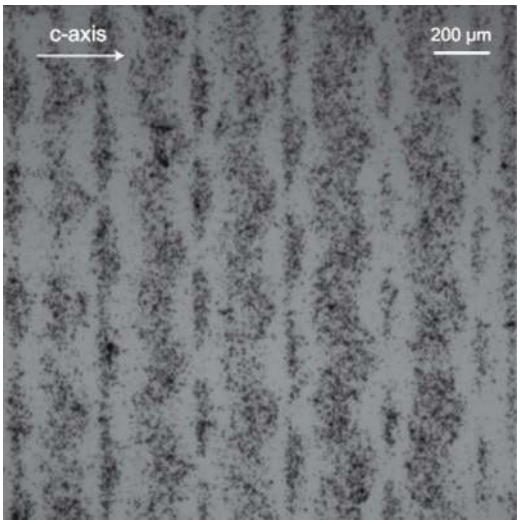

FIG. 15. 2D pattern of graphite particles deposited on the surface of a *x*-cut $LiNbO_3$:Fe crystal illuminated with a mosaic structure of triangles. Reprinted with permission from Esseling *et al.*, Opt. Express **18**, 17404 (2010). Copyright 2010 Optical Society of American.

D. Persistence and reconfiguration of particle patterns

The patterns are stable at room temperature (RT) in accordance with the persistence of the photorefractive effect. Although the PV field only operates during illumination, the liberated electronic charges become finally trapped at acceptor Fe^{3+} sites. The space-charge fields persist over a long time that depends on the dark conductivity of the sample, i.e., on the doping level and oxidation-reduction state ($[Fe^{2+}]/[Fe^{3+}]$). Typical times are in the range of minutes-months. However, the patterns can be erased either by uniform illumination or by heating the substrate above RT. Therefore, one has a means to record sequentially different patterns on the same crystal surface and so the patterning method offers reconfigurability. A first demonstration of these reconfiguration capabilities has been very recently reported.[72] In this work, two periodic particle patterns with different orientations with regard to the polar axis (45° and 90°) have been alternatively deposited as illustrated in Figure 17(a). After PV field recording by holographic illumination, particle deposition on the substrate and homogeneous light erasure to remove particles are successfully applied several times. The resulting particle patterns are shown in Figures 17(b)–17(d) demonstrating the reconfiguration capability. The suitability to apply the reconfiguration processes in opto-fluidic channels is also proved.

FIG. 16. 2D pattern obtained from a suspension of charged particles deposited by electrophoretic forces on a *z*-cut lithium niobate crystal; the inset shows the corresponding light pattern. The microscope image shows that charged particles adhere well to the previously illuminated regions without any anisotropy. Reprinted with permission from Appl. Phys. Lett. **103**, 061115 (2013). Copyright 2013 AIP Publishing LLC.

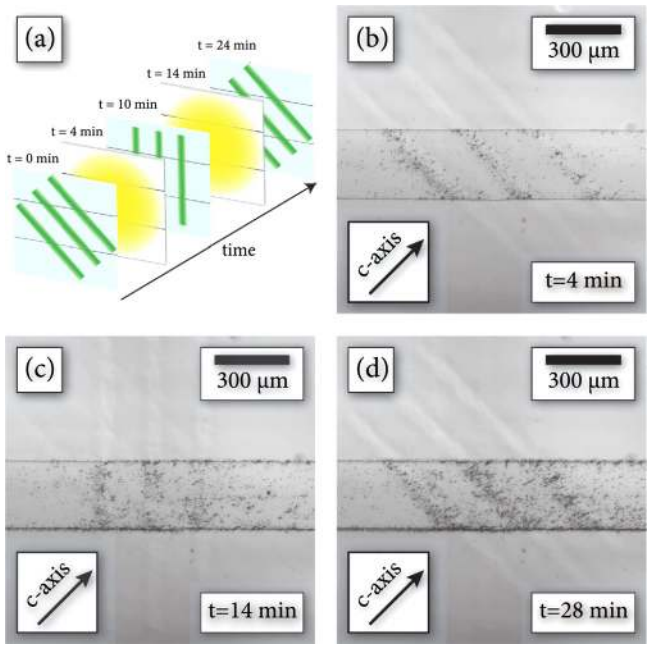

FIG. 17. Sequential switching of virtual electrodes in order to trap graphite particles in a microchannel: (a) Illustration of the writing and erasure sequence (including time scale) and (b)–(d) corresponding particle arrangements. Reprinted with permission from Glaesener *et al.*, Opt. Lett. **37**, 3744 (2012). Copyright 2012 Optical Society of American.

On the other hand, diverse fixing[73] techniques for the recorded holographic PR gratings have been developed, which permit the preparation of permanent patterns versus thermal fading and homogeneous illumination. In fact, lifetimes in the dark reach the scale of several years.[74,75]

V. COMPARISON WITH OTHER ALTERNATIVE TECHNIQUES USING $LiNbO_3$

As mentioned in the Introduction, a few alternative techniques based on related physical principles have been proposed for particle patterning on the surface of ferroelectrics crystals such as $LiNbO_3$. They differ from PV tweezers in the way used to generate the electric field patterns responsible for particle manipulation. One approach takes advantage of the electric field distribution generated under UV illumination at the surface of a patterned undoped $LiNbO_3$, consisting of domains having alternative poling vectors and so alternative surface charges. The corresponding field distribution, showing high peak values at the domain boundaries, have been calculated[17] and can be used for patterning of nanoparticles through two different strategies. One uses the DEP and EP forces generated by those field patterns as in the PV tweezers to decorate the domain boundaries.[76] The other

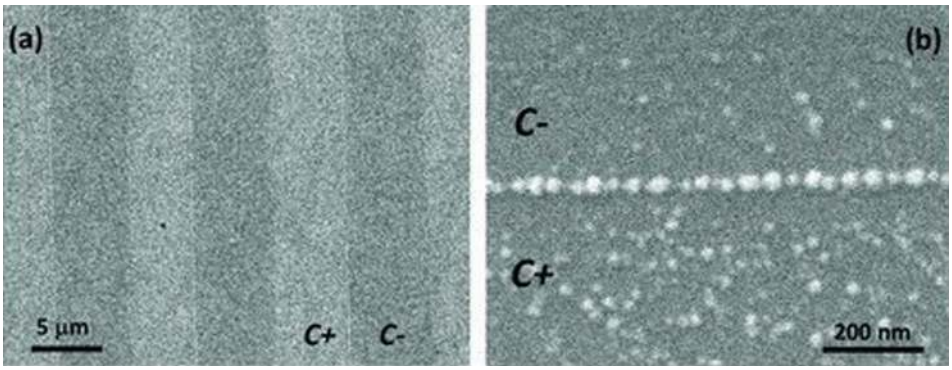

FIG. 18. (a) SEM image of the surface of a Nd^{3+} doped PPLN crystal after selective photochemical deposition of Ag NPs; dark regions correspond to $c-$ domain surfaces with a low Ag NP density; light regions are $c+$ domain surfaces with a higher density of Ag. (b) Higher resolution SEM image showing a domain boundary on which a chain of Ag nanoparticles has been formed. Reprinted with permission from Yraola *et al.*, Adv. Mater. **25**, 910 (2013). Copyright 2013 John Wiley and Sons.

approach is based on the use of domain-specific reactions and it is designated as ferroelectric lithography.[33,77,78] The fields are used to induce localized chemical reactions, nanopatterned surface functionalization, and photoinduced formation of metallic nanostructures. In one relevant example, patterns of silver nanoparticles are deposited on the PPLN surface from an $AgNO_3$ solution under UV-light exposure with photon energy higher than the band gap (~3.9 eV) (see Figure 18). The photo-induced process produces electron-hole carriers that migrate to the surface to reduce Ag^+ and it results in preferential Ag^0 deposition along the domain boundaries, where the field is higher. Then, the reduced silver atoms nucleate to form larger clusters and nano-particles. A good control of the technique has been already reached[35,77,78] as illustrated in Figure 18. One should note that a similar procedure could operate using the PV induced field patterns.

A related method uses a ferroelectric domain structure that is heated to induce the evanescent electric field through pyroelectric effect.[22,49] The latter effect depends on the temperature dependence of the spontaneous polarization of a ferroelectric material, like $LiNbO_3$.[79,80] The basic pyroelectric equation describing the pyroelectric current generated by a temperature change δT writes

$$J_{pyro} = p\frac{\delta T}{\delta t}, \tag{19}$$

p being the pyroelectric coefficient.[81] Under open circuit conditions, this current can generate high electric fields at the domain boundaries,[82] which allow particle trapping and patterning via dielectrophoretic forces. The method has been used for assembling nanoparticles and nanotubes through electrode-free dielectrophoresis to develop complex functional capabilities.[49,83] Reported applications in the biological area include self-assembly of yeast cells as illustrated in Figure 19[49] and disinfection of aqueous solutions containing nano- and micro-crystalline powders of lithium niobate and lithium tantalite.[48]

Main advantages of PV tweezers over these alternative methods are the *flexibility* of the light patterns to induce particle patterning, the reconfiguration capabilities, and the simpler methodology. Anyhow, a deeper comparative analysis of these effects is in order. On the other hand, a possible disadvantage of PV fields is the need of substrate doping to have a large PV effect under visible light.

VI. APPLICATIONS OF PV TWEEZERS

The results and analyses presented in this review suggest a large span of possibilities for application although only a few ones have been demonstrated so far.

For ***Life Sciences***, including biology, biomedicine, and environmental sciences, the possible use of the PV fields is quite open, mainly in connection with suitable microfluidic devices.[49,84] The miniaturization of fluid systems to create microfluidic devices has opened a vast landscape in both science and technology. For biology and biomedicine, lab-on-chip devices with narrow channels of around 10 μm offer interesting possibilities for cell manipulation enabling the diagnosis of certain pathologies. A good example of this strategy is provided by the work of Bao and Lu,[85] which uses microscale silica beds in a microfluidic channel to stop *Escherichia coli* cells in solution. Subsequent electrical pulses rapidly lyse the cells and release intracellular proteins from them. Although in that work the electric fields are produced by conventional methods, the use of the PV method would offer a promising alternative. In fact, more recently, the PV strategy has been already applied to basic microfluidic experiments.[27,69,86] In particular, in Refs. 69 and 86, the authors implemented a two steps procedure. In a first step, a microfluidic channel is fabricated on a polydimethilsiloxane (PDMS) film deposited on a $LiNbO_3$ substrate through the photorefractive effect using a SLM for patterning the illumination. In a second stage, the PV effect is again used to produce nanoparticle trapping as described for the PV tweezers. A rather different specific application of the PV method in biomedicine to kill tumor cells cultivated on the surface of a Fe:$LiNbO_3$ sample by using visible light has been reported.[23] These results are illustrated in Figure 20, taken from that paper, where the population of alive and death cells versus the illumination time is plotted. Similarly, the use of the high PV fields achieved by illumination has been proposed to kill bacteria in polluted environments.[87] For this type of applications, one should also mention that the pyroelectric fields developed in micro- and nano-crystalline $LiNbO_3$ has been successfully used as a disinfection mechanism by killing *E. coli* bacteria in aqueous solution.[48] Finally, another related applications manipulate different kind of bio-objects using PV tweezers. For instance, in Ref. 88, alive bacteria are immobilized on the PV substrate and oriented mainly along the PV field (see Figure 21) and in Ref. 89 massive trapping and patterning of spores and pollen grains are reported.

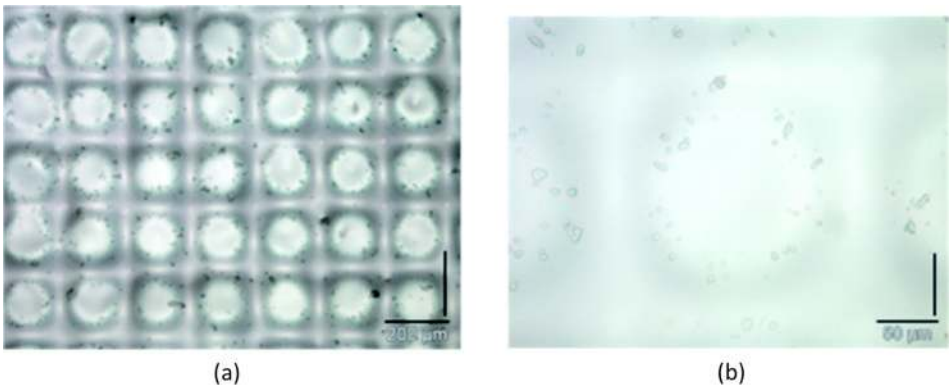

FIG. 19. (a) Large and (b) magnified view of yeast cells trapped via the pyroelectric effect on the surface of a hexagon square array PPLN pattern (period of 200 μm). Reprinted with permission from Grilli *et al.*, RSC Adv. **4**, 2851 (2014). Copyright 2014 The Royal Society of Chemistry.

For ***Photonics and Integrated Optics***, a relevant and quite feasible application to photonic technologies consists in the fabrication of masks and diffractive optical elements that can be reconfigurable, such as holographic gratings, Fresnel lenses, and Bragg reflectors for laser technologies. These devices would be simply based on the holographic patterns already achieved with metal nanoparticles.[26,52] In this case, one could benefit from the enhancement scattering effects associated to plasmon resonances in nanoparticles and nanowires. On the other hand, a recent work[61] has extended the operation of the PV patterning method to waveguide substrates on $LiNbO_3$, which can be fabricated by a variety of techniques.[90,91] This opens the way to fabricate micro- and nanostructures for integrated optics components such as holographic coupling devices and Bragg reflectors for waveguide lasers. A different relevant application[61] has used proton exchanged and swift heavy ion irradiation waveguides on Fe:$LiNbO_3$ to visualize the photorefractive optical damage along propagation of a light beam through the waveguides. Aside from illustrating the good capabilities of the waveguide configuration for trapping and patterning of nanoparticles (see Figure 22), the image reveals the development of noise scattering gratings responsible of photorefractive beam fanning and degradation.[92,93] Moreover, a main advantage of the waveguide configuration is a much faster response time in comparison to bulk substrates.

In ***Nanoelectronics***, miniaturization of electronic devices requires the development of metal nanowires as interconnecting components at the nano-scale. The PV methods here described may provide a possible solution. Moreover, linear arrays of metal nanoparticles may lead to the fabrication of nano-optical circuits for optical confinement at the nanoscale.

Finally, there are, also, other fields, where the PV method may be useful such as for ***sensors devices***. For example, the evanescent PV fields responsible for the trapping and patterning effects can be used as a charge sensor for the trapped particles[70] as illustrated in Figure 23.

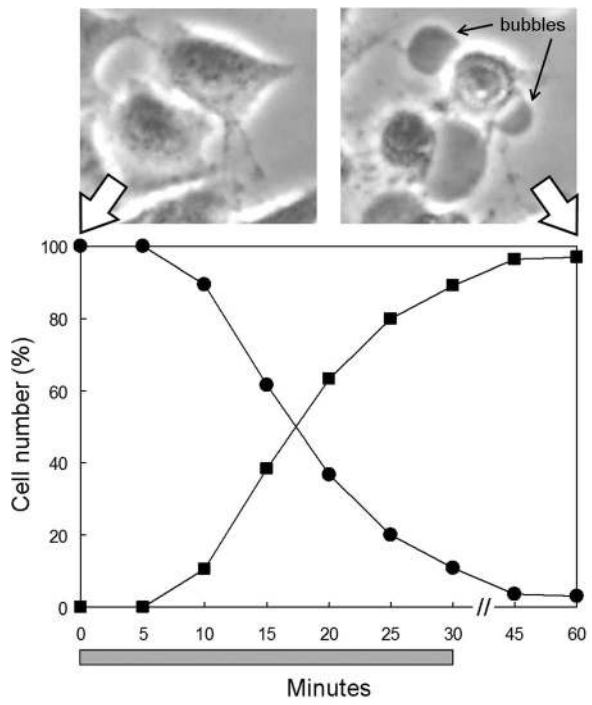

FIG. 20. Evolution of the percentage of Hella cells with normal morphology (circles) and necrotic morphology (squares) cultured on the Fe:$LiNbO_3$ crystal surface and exposed during 30 min to light (546 nm, 66.6 J/m^2). Reprinted with permission from Blázquez-Castro *et al.*, Photochem. Photobiol. Sci. **10**, 956 (2011). Copyright 2011 The Royal Society of Chemistry.

VII. SUMMARY AND OUTLOOK

The review has offered an up-to-date perspective on the state of the art for the novel trapping and patterning method of nanoparticles, based on the PV properties of $LiNbO_3$. The

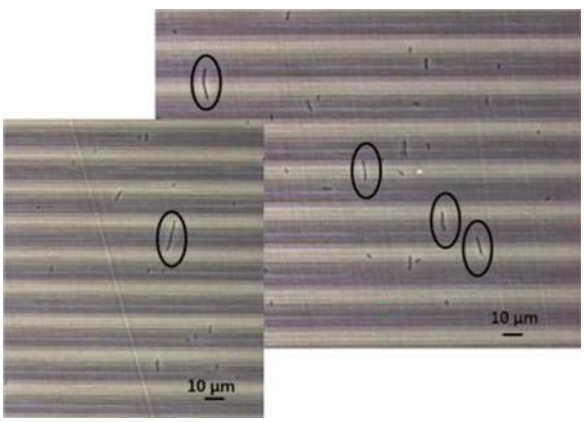

FIG. 21. Images of *E. coli* bacteria chains aligned perpendicular to the photorefractive grating planes recorded in Fe:$LiNbO_3$. Chains longer than 10 μm are marked. The grating period is 25 μm. Reprinted with permission from Miccio *et al.*, Opt. Laser Eng. (published online). Copyright 2015 Elsevier.

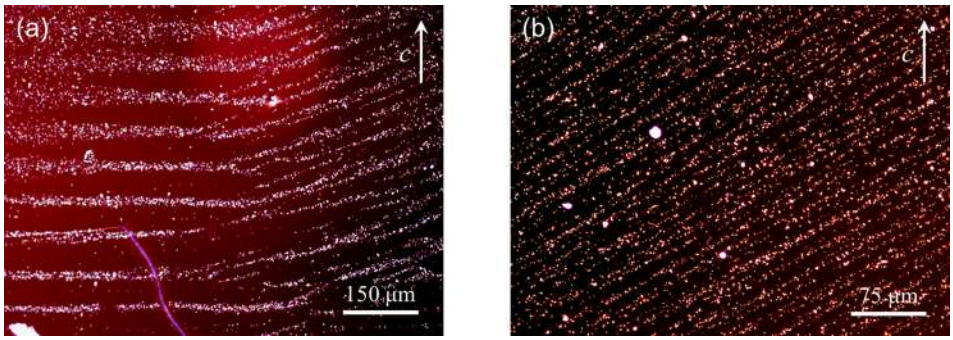

FIG. 22. (a) Microphotograph of patterns obtained with Al nano-particle deposited from a hexane suspension after sinusoidal light illumination ($\Lambda = 50\,\mu$m) on an optical SHI waveguide that exhibits photorefractive optical damage. (b) Pattern corresponding to the same sample but showing a region centered on a longer propagation length. Reprinted with permission from Jubera *et al.*, Opt. Lett. **39**, 649 (2014). Copyright 2014 Optical Society of American.

method is still young and under development, so that only a few of its promising capabilities have been exploited.

The main output of our work is that one can use the high PV effect of $LiNbO_3$ to trap and arrange micro/nanometric particles according to patterns that can be governed by imposed light intensity profiles. The so called PV tweezers allow combining the imaging (parallel) massive capabilities of light with the nonlinear photorefractive response of $LiNbO_3$ and other non-centrosymmetric crystals. The method offers an outstanding flexibility, since neither electrodes nor voltage suppliers are required and patterns can be easily erased and reconfigurated. 1D as well as 2D arrangements have been already demonstrated and, in principle, simple 3D structures might be also obtained taking advantage of the spatial range of the electrophoretic and dielectrophoretic forces in the direction normal to the PV substrate.

Although the basic model to describe the PV patterning effects is well understood, its application to the very promising perpendicular configuration is still at a first stage. Moreover, there are still many basic questions that should be clarified such as the effect of the competition of electrophoresis and dielectrophoresis that can appear in some experiments or the contribution of the interaction between polarized particles. So far, the minimum periods achieved are of a few micrometers although further optimization of the experimental procedures should allow reaching submicrometric periods much more interesting for applications in nanotechnology. Moreover, the dynamic effects associated to variable light illumination or moving light patterns have been scarcely investigated so far, even they may have interesting applications for manipulation of nano-objects. For example, one could shift the trapping patterns by moving the substrate or, alternatively, by running the light fringes profile introducing a variable phase-shift on one of the interfering beams. Another interesting route to explore is the combination of photovoltaic and pyroelectric effects in mono- or poly-domain substrates in order to expand and/or optimize the capabilities of trapping and patterning. As for applications, although a few ones have been already demonstrated and reviewed here, the potential of the method still remains mostly unexplored. New applications in the fields of photonics, nano-, or biotechnology such as those already suggested (generation of plasmonic nanostructures, fabrication of diffractive devices, or patterning and manipulation of bio-objects, etc.) should be developed in the near future. It is expected that this review may stimulate research activity in those directions.

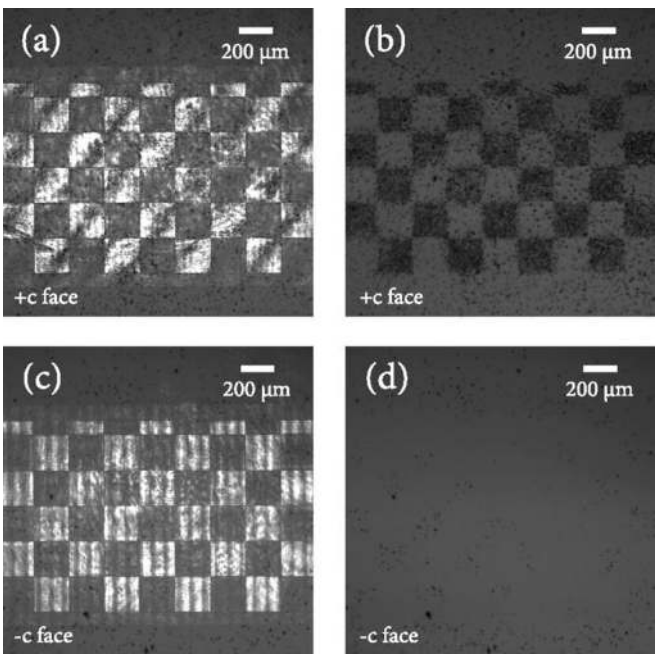

FIG. 23. A z-cut $LiNbO_3$ substrate as charge sensor: (a) illumination of $+c$ face with a binary square pattern and subsequent adhesion (b) of positively charged graphite spheres suspended in Novec 7300 to the illuminated regions; (c) illumination of $-c$ face with the same pattern resulting in (d) repulsion of positively charged particles from the high intensity regions. Reprinted with permission from Appl. Phys. Lett. **103**, 061115 (2013). Copyright 2013 AIP Publishing LLC.

ACKNOWLEDGMENTS

This work was supported by Project Nos. MAT2011-28379-C03 and MAT2014-57704-C03.

[1]D. G. Grier, "A revolution in optical manipulation," Nature **424**, 810 (2003).
[2]P. Y. Chiou, A. T. Ohta, and M. C. Wu, "Massively parallel manipulation of single cells and microparticles using optical images," Nature **436**, 370 (2005).
[3]M. Maragò, P. H. Jones, P. G. Gucciardi, G. Volpe, and A. C. Ferrari, "Optical trapping and manipulation of nanostructure," Nat. Nanotech. **8**, 807 (2013).
[4]T. M. Squires and S. R. Quake, "Microfluidics: Fluid physics at the nanoliter scale," Rev. Mod. Phys. **77**, 977 (2005).
[5]A. M. Baró, R. Miranda, J. Alamán, N. García, G. Binnig, H. Rohrer, Ch. Gerber, and J. L. Carrascosa, "Determination of surface topography of biological specimens at high resolution by scanning tunnelling microscopy," Nature **315**, 253 (1985).
[6]F. Ritort, "Single-molecule experiments in biological physics: methods and applications," J. Phys. Condens. Matter **18**, R531 (2006).

[7]M. H. Korayem and M. Zakeri, "Sensitivity analysis of nanparticles pushing critical conditions in 2-D controlled nanomanipulation based on AFM," Int. J. Adv. Manuf. Technol. **41**, 714–726 (2009).

[8]A. Ashkin, "Acceleration and trapping of particles by radiation pressure," Phys. Rev. Lett. **24**, 156 (1970).

[9]A. Ashkin, "Forces of a single-beam gradient laser trap on a dielectric sphere in the ray optics regime," Biophys. J. **61**, 569 (1992).

[10]M. Woerdemann, S. Gläsener, F. Hörner, A. Devaux, L. De Cola, and C. Denz, "Dynamic and reversible organization of zeolite L crystals induced by holographic optical tweezers," Adv. Mater. **22**, 4176 (2010).

[11]H. Pohl, *Dielectrophoresis: The Behavior of Neutral Matter in Nonuniform Electric Fields* (Cambridge University Press, 1978).

[12]T. B. Jones, *Electromechanics of Particles* (Cambridge University Press, 1995).

[13]K. D. Hermanson, S. Lumsdon, J. P. Williams, E. Kaler, and O. D. Velev, "Dielectrophoretic assembly of electrically functional microwires from nanoparticle suspensions," Science **294**, 1082 (2001).

[14]P. Gascoyne and J. Vykoukal, "Particle separation by dielectrophoresis," Electrophoresis **23**, 1973 (2002).

[15]A. Kadaksham, P. Singh, and N. Aubry, "Dielectrophoresis of nanoparticles," Electrophoresis **25**, 3625 (2004).

[16]D. Li and D. A. Bonnell, "Controlled patterning of ferroelectric domains: Fundamental concepts and applications," Annu. Rev. Mater. Res. **38**, 351 (2008).

[17]P. Mokrý, M. Marvan, and J. Fousek, "Patterning of dielectric nanoparticles using dielectrophoretic forces generated by ferroelectric polydomain films," J. Appl. Phys. **107**, 094104 (2010).

[18]V. Ya. Shur, A. R. Akhmatkhanov, and I. S. Baturin, "Micro and nanodomain engineering in lithium niobate," Appl. Phys. Rev. **2**, 040604 (2015).

[19]J. L. Giocondini and G. Rohrer, "Spatially selective photochemical reduction of silver on the surface of ferroelectric barium titanate," Chem. Mater. **13**, 241 (2001).

[20]S. V. Kalinin, D. A. Bonnell, T. Alvarez, X. Lei, Z. Hu, and J. H. Ferris, "Atomic polarization, charge compensation, and local reactivity on ferroelectric surfaces: A new route toward complex nanostructures," Nano Lett. **2**, 589 (2002).

[21]J. N. Hanson, B. J. Rodriguez, R. J. Nemanich, and A. Gruverman, "Fabrication of metallic nanowires on a ferroelectric template via photochemical reaction," Nanotechnology **17**, 4946 (2006).

[22]S. Grilli and P. Ferraro, "Dielectrophoretic trapping of suspended particles by selective pyroelectric effect in lithium niobate crystals," Appl. Phys. Lett. **92**, 232902 (2008).

[23]A. Blázquez-Castro, J. C. Stockert, B. López-Arias, A. Juarranz, F. Agulló-López, A. García-Cabañes, and M. Carrascosa, "Tumour cell death induced by the bulk photovoltaic effect of $LiNbO_3$:Fe under visible light irradiation," Photochem. Photobiol. Sci. **10**, 956 (2011).

[24]S. S. Sarkisov, M. J. Curley, N. V. Kukhtarev, A. Fields, G. Adamovsky, C. C. Smith, and L. E. Moore, "Holographic surface gratings in iron-doped lithium niobate," Appl. Phys. Lett. **79**, 901 (2001).

[25]H. A. Eggert, F. Y. Kuhnert, K. Buse, J. R. Adleman, and D. Psaltis, "Trapping of dielectric particles with light-induced space-charge fields," Appl. Phys. Lett. **90**, 241909 (2007).

[26]X. Zhang, J. Wang, B. Tang, X. Tan, R. A. Rupp, L. Pan, Y. Kong, Q. Sun, and J. Xu, "Optical trapping and manipulation of metallic micro/nanoparticles via photorefractive crystals," Opt. Express **17**, 9981 (2009).

[27]M. Esseling, F. Holtmann, M. Woerdemann, and C. Denz, "Two-dimensional dielectrophoretic particle trapping in a hybrid crystal/PDMS-system," Opt. Express **18**, 17404 (2010).

[28]*Photorefractive Materials and Their Applications I*, edited by P. Günter and J. P. Huignard (Springer, New York, 2006).

[29]*Photorefractive Materials and Their Applications II*, edited by P. Günter and J. P. Huignard (Springer, New York, 2007).

[30]B. Sturmann and V. Fridkin, *Photovoltaic and Photorefractive Effects in Noncentosymetric Materials* (Gordon and Breach Science Publishers, Philadelphia, 1992).

[31]J. Villarroel, H. Burgos, A. García-Cabañes, M. Carrascosa, A. Blázquez-Castro, and F. Agulló-López, "Photovoltaic versus optical tweezers," Opt. Express **19**, 24320 (2011).

[32]N. Kukhtarev, T. Kukhtareva, and J. Wang, "Photoinduced electrokinetic redistribution of nano/microparticles during holographic grating recording in the ferroelectric crystal," Proc. SPIE **8120**, 81200A (2011).

[33]X. Liu, K. Kitamura, K. Terabe, H. Hatano, and N. Ohashi, "Photocatalytic nanoparticle deposition on $LiNbO_3$ nanodomain patterns via photovoltaic effect," Appl. Phys. Lett. **91**, 044101 (2007).

[34]X. Liu, F. Ohuchi, and K. Kitamura, "Patterning of silver nanoparticles on visible light-sensitive Mn-doped lithium niobate photogalvanic crystals," Appl. Phys. Lett. **99**, 053102 (2011).

[35]Y. Sun, B. Eller, and R. Nemanich, "Photo-induced Ag deposition on periodically poled lithium niobate: Concentration and intensity dependence," J. Appl. Phys. **110**, 084303 (2011).

[36]L. Arizmendi, "Photonic applications of lithium niobate crystals," Phys. Status Solidi A **201**, 253 (2004).

[37]F. Agullo-Lopez, J. M. Cabrera, and F. Agulló-Rueda, *Electrooptics: Phenomena, Materials and Applications* (Academic Press, London, 2006).

[38]E. M. de Miguel, J. Limeres, M. Carrascosa, and L. Arizmendi, "Study of developing thermal fixed holograms in lithium niobate," J. Opt. Soc. Am. B **17**, 1140 (2000).

[39]E. Krätzig and H. Kurz, "Spectroscopic investigation of photovoltaic effects in doped $LiNbO_3$," J. Electrochem. Soc. **124**, 131–134 (1977).

[40]F. Lüdtke, N. Waasem, K. Buse, and B. Sturman, "Light-induced charge-transport in undoped $LiNbO_3$ crystals," Appl. Phys. B **105**, 35 (2011).

[41]J. Villarroel, J. Carnicero, F. Lüedtke, M. Carrascosa, A. García-Cabañes, J. M. Cabrera, A. Alcazar, and B. Ramiro, "Analysis of photorefractive optical damage in lithium niobate: Application to planar waveguides," Opt. Express **18**, 20852 (2010).

[42]F. Lüedtke, J. Villarroel, A. García-Cabañes, K. Buse, and M. Carrascosa, "Correlation between photorefractive index changes and optical damage thresholds in *z*-cut proton-exchanged-$LiNbO_3$ waveguides," Opt. Express **17**, 658 (2009).

[43]M. Imlau, "Optical nonlinearities of small polarons in lithium niobate and their impact on frequency conversion using (ultra-) short laser pulses," Appl. Phys. Rev. **2**, 040606 (2015).

[44]O. F. Schirmer, "X-ray photovoltaic effect in undoped $LiNbO_3$ and its correlation with ESR," J. Appl. Phys. **50**, 3404 (1979).

[45]V. Fridkin, G. Dalba, P. Fornasini, Y. Soldo, F. Roccac, and E. Burattini, "The bulk photovoltaic effect in $LiNbO_3$, crystals under X-ray synchrotron radiation," Ferroelectr. Lett. **16**, 1 (1993).

[46]G. Dalba, Y. Soldo, F. Rocca, V. M. Fridkin, and Ph. Sainctavit, "Giant bulk photovoltaic effect under linearly polarized X-ray synchrotron radiation," Phys. Rev. Lett. **74**, 988 (1995).

[47]Y. Sun and R. J. Nemanich, "Photoinduced Ag deposition on periodically poled lithium niobate: Wavelength and polarization screening dependence," J. Appl. Phys. **109**, 104302 (2011).

[48]E. Gutmann, A. Benke, K. Gerth, H. Böttcher, E. Mehner, C. Klein, U. Krause-Buchholz, U. Bergmann, W. Pompe, and D. Meyer, "Pyroelectrocatalytic disinfection using the pyroelectric effect of nano- and microcrystalline $LiNbO_3$ and $LiTaO_3$ particles," J. Phys. Chem. C **116**, 5383 (2012).

[49]S. Grilli, S. Coppola, G. Nasti, V. Vespini, G. Gentile, V. Ambrogi, C. Carfagna, and P. Ferraro, "Hybrid ferroelectric polymer micro fluidic device for dielectrophoretic self-assembling of nanoparticles," RSC Adv. **4**, 2851 (2014).

[50]A. M. Glass, D. Von der Linde, and T. Negran, "High voltage bulk photovoltaic effect and the photorefractive process in $LiNbO_3$," Appl. Phys. Lett. **25**, 233 (1974).

[51]F. Agulló-López, G. F. Calvo, and M. Carrascosa, *Photorefractive Materials and Applications* (Springer, New York, 2006), Chap. 3.

[52]H. Burgos, M. Jubera, J. Villarroel, A. García-Cabañes, F. Agulló-López, and M. Carrascosa, "Role of particle anisotropy and deposition method on the patterning of nano-objects by the photovoltaic effect in $LiNbO_3$," Opt. Mater. **35**, 1700 (2013).

[53]C. Arregui, J. B. Ramiro, A. Alcázar, A. Méndez, H. Burgos, A. García-Cabañes, and M. Carrascosa, "Optoelectronic tweezers under arbitrary illumination patterns: Theoretical simulations and comparison to experiment," Opt. Express **22**, 29099 (2014).

[54]M. Aguilar, M. Carrascosa, F. Agulló-López, and L. F. Magaña, "Holographic recording in photorefractive thin films: Edge effects," J. Appl. Phys. **78**, 4840 (1995).

[55]L. Solymar, M. Aguilar, and F. Agulló-López, "Unified two dimensional model for grating dynamics in photorefractive crystals," J. Appl. Phys. **80**, 1268 (1996).

[56]E. Serrano, V. López, M. Carrascosa, and F. Agulló-López, "Steady-state photorefractive gratings in $LiNbO_3$ for strong light modulation depths," J. Quantum Electron. **30**, 875 (1994).

[57]E. Serrano, M. Carrascosa, and F. Agulló-López, "Analytical and numerical study of photorefractive kinetics at high modulation depths," J. Opt. Soc. Am. B **13**, 2587 (1996).
[58]G. Videen, "Light scattering from a particle on or near a perfectly conducting surface," Opt. Commun. **115**, 1 (1995).
[59]C. Arregui, J. B. Ramiro, A. Alcázar, A. Mendez, J. F. Muñoz-Martínez, and M. Carrascosa, "Comparative theoretical analysis between parallel and perpendicular geometries for 2D particle patterning in photovoltaic ferroelectric substrates," J. Eur. Opt. Soc. (Rapid Publication) **10**, 15026 (2015).
[60]M. Esseling, A. Zaltron, N. Argiolas, G. Nava, J. Imbrock, I. Cristiani, C. Sada, and C. Denz, "Highly reduced iron-doped lithium niobate for optoelectronic," Appl. Phys. B **113**, 191 (2013).
[61]M. Jubera, A. García-Cabañes, J. Olivares, A. Alcazar, and M. Carrascosa, "Particle trapping and structuring on the surface of $LiNbO_3$:Fe optical waveguides using photovoltaic fields," Opt. Lett. **39**, 649 (2014).
[62]J. Carnicero, A. Méndez, M. Carrascosa, and A. García-Cabañes, "Photorefractive α-phase PE:$LiNbO_3$ waveguides prepared on iron doped substrates," Ferroelectrics **352**, 86 (2007).
[63]M. Jubera, A. García-Cabañes, M. Carrascosa, J. Olivares, and F. Lüedtke, "Characterization and inhibition of photorefractive optical damage of swift heavy ion irradiation waveguides in $LiNbO_3$," J. Opt. Soc. Am. B **29**, 3000 (2012).
[64]M. Esseling, S. Glasener, F. Volonteri, and C. Denz, "Opto-electric particle manipulation on a bismuth silicon oxide crystal," Appl. Phys. Lett. **100**, 161903 (2012).
[65]J. Matarrubia, A. García-Cabañes, J. L. Plaza, F. Agulló-López, and M. Carrascosa, "Optimization of particle trapping and patterning via photovoltaic tweezers: Role of light modulation and particle size," J. Phys. D **47**, 265101 (2014).
[66]N. Kukhtarev, T. Kukhtareva, and F. Okafor, "Optical trapping/modification of nano-(micro)particles by gradient and photorefractive forces during laser illumination," Proc. SPIE **7781**, 778110 (2010).
[67]S. A. Torres-Hurtado, B. M. Villegas-Vargas, N. Korneev, J. C. Ramirez-San-Juan, and R. Ramos-Garcia, "Optical trapping and optical micromanipulation," Proc. SPIE **8458**, 845825 (2012).
[68]M. Carrascosa, H. Burgos, J. Matarrubia, M. Jubera, A. Garcia-Cabañes, and F. Agulló-López, "Photoelectric trapping and pattering of micro- and nano-particles on iron doped $LiNbO_3$," in *Proceedings of OPTOEL13* (2013), pp. 415–420.
[69]L. Miccio, P. Memmolo, S. Grilli, and P. Ferraro, "All-optical microfluidic chips for reconfigurable dielectrophoretic trapping through SLM light induced patterning," Lab Chip **12**, 4449 (2012).
[70]M. Esseling, A. Zaltron, C. Sada, and C. Denz, "Charge sensor and particle trap based on *z*-cut lithium niobate," Appl. Phys. Lett. **103**, 061115 (2013).
[71]J. F. Muñoz-Martínez, I. Elvira, M. Jubera, A. García-Cabañes, J. Bruno Ramiro, C. Arregui, and M. Carrascosa, "Efficient photo-induced dielectrophoretic particle trapping on Fe:$LiNbO_3$ for arbitrary two dimensional patterning," Opt. Mater. Express **5**, 1137 (2015).
[72]S. Glaesener, M. Esseling, and C. Denz, "Multiplexing and switching of virtual electrodes in optoelectronic tweezers based on lithium niobate," Opt. Lett. **37**, 3744 (2012).
[73]M. Carrascosa, L. Arizmendi, and M. J. Cabrera, *Photorefractive Materials and Their Applications* (Springer, New York, 2006), Chap. 12.
[74]L. Arizmendi, E. M. de Miguel-Sanz, and M. Carrascosa, "Lifetimes of thermally fixed holograms in $LiNbO_3$:Fe crystals," Opt. Lett. **23**, 960 (1998).
[75]E. M. de Miguel-Sanz, M. Carrascosa, and L. Arizmendi, "Effect of the oxidation state and hydrogen concentration on the lifetime of thermally fixed holograms in $LiNbO_3$:Fe," Phys. Rev. B **65**, 165101 (2002).
[76]C. Ke, X. Wang, X. P. Hu, S. N. Zhu, and M. Qi, "Nanoparticle decoration of ferroelectric domain patterns in $LiNbO_3$ crystal," J. Appl. Phys. **101**, 064107 (2007).
[77]D. Li and A. Bonnell, "Ferroelectric lithography," Ceram. Int. **34**, 157 (2008).
[78]E. Yraola, P. Molina, J. L. Plaza, M. O. Ramírez, and L. E. Bausá, "Spontaneous emission and nonlinear response enhancement by silver nanoparticles in a Nd^{3+}-doped periodically poled $LiNbO_3$ laser crystal," Adv. Mater. **25**, 910 (2013).
[79]R. W. Whatmore, "Pyroelectric devices and materials," Rep. Prog. Phys. **49**, 1335 (1986).
[80]G. Rosenman, D. Shur, Y. E. Krasik, and A. Dunaevsky, "Electron emission from ferroelectrics," J. Appl. Phys. **88**, 6109 (2000).
[81]R. S. Weis and T. K. Gaylord, "Lithium niobate: Summary of physical properties and crystal structure," Appl. Phys. A **37**, 191 (1985).
[82]K. Kitamura, H. Hatano, S. Takekawa, and D. Schutze, "Large pyroelectric effect in Fe-doped lithium niobate induced by a high-power short-pulse laser," Appl. Phys. Lett. **97**, 082903 (2010).
[83]S. Grilli, S. Coppola, V. Vespini, V. Pagliarulo, G. Nasti, C. Carfagna, and P. Ferraro, "One-step fabrication of free-standing flexible membranes reinforced with self-assembled arrays of carbon nanotubes," Appl. Phys. Lett. **105**, 153101 (2014).
[84]P. Tabeling, *Introduction to Microfluidics* (OUP, Oxford, 2005).
[85]N. Bao and C. Lu, "A microfluidic device for physical trapping and electrical lysis of bacterial cells," Appl. Phys. Lett. **92**, 214103 (2008).
[86]L. Miccio, M. Paturzo, A. Finizio, and P. Ferraro, "Light induced patterning of poly (dimethylsiloxane) microstructures," Opt. Express **18**, 10947 (2010).
[87]A. Blazquez, J. C. Stockert, M. Carrascosa, A. García-Cabañes, and F. Agulló-López, Spanish patent ES2380033.
[88]L. Miccio, V. Marchesano, M. Mugnano, S. Grilli, and P. Ferraro, "Light induced DEP for immobilizing and orienting *Escherichia coli* bacteria," Opt. Laser Eng. (published online).
[89]M. Carrascosa, A. Garcia-Cabañes, M. Jubera, I. Elvira, H. Burgos, J. L. Bella, F. Agulló-López, J. F. Muñoz-Martinez, and A. Alcazar, "Photovoltaic tweezers: An emergent tool for applications in nano and bio-technology," Proc. SPIE **9529**, 95290Q (2015).
[90]D. Kip and M. Wesner, *Photorefractive Materials and their Applications I* (Springer, New York, 2006), Chap. 10.
[91]M. Bazzan, C. Sada *et al.*, "Optical waveguides in lithium niobate: Recent developments and applications" Appl. Phys. Rev. **2**, 040603 (2015).
[92]J. Feinberg, "Asymmetric self-defocusing of an optical beam from the photorefractive effect," J. Opt. Soc. Am. **72**, 46 (1982).
[93]M. Carrascosa, J. Villarroel, J. Carnicero, A. García-Cabañes, and J. M. Cabrera, "Understanding light intensity thresholds for catastrophic optical damage in $LiNbO_3$," Opt. Express **16**, 115 (2008).